

## Supporting Information

### *Importance of Lithium Coordination Structure to Lithium-Ion Transport in Polyether Electrolytes with Cyanoethoxy Side Chains: An Experimental and Theoretical Approach*

*Riho Matsuoka<sup>1</sup>, Masayuki Shibata<sup>1</sup>, Kousuke Matsuo<sup>1</sup>, Ryansu Sai<sup>1</sup>, Hiromori Tsutsumi<sup>1</sup>, Kenta Fujii<sup>1\*</sup>, and Yu Katayama<sup>1\*</sup>*

*<sup>1</sup> Department of Applied Chemistry, Graduate School of Sciences and Technology for Innovation, Yamaguchi University, Tokiwadai, Ube, 755-8611, Japan*

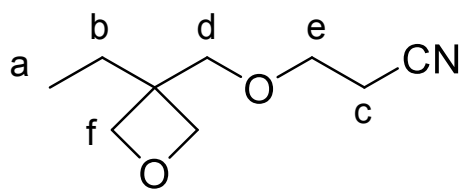
## Monomer synthesis

3-(2-cyanoethoxymethyl)-3-ethyloxetane (CEO) was synthesized from 3-ethyl-3-hydroxymethyloxetane (EHO) by Michael addition based on a reported procedure.<sup>4,5</sup> EHO (57 mL, 0.500 mol, Tokyo Chemical Industry Co., Ltd.) was mixed with acrylonitrile (60 mL, 0.915 mol, Wako Pure Chemical Co.) in ultrapure water (25 mL, Elix-UV3, Nihon Millipore K.K.) containing a 20% tetraethylammonium hydroxide solution (6.5 mL, Wako Pure Chemical Co.) as a catalyst, and the mixture was stirred at room temperature for 17 h. The reaction mixture was extracted with chloroform and subsequently washed with water. After the solution was dehydrated with magnesium sulfate (Wako Pure Chemical Co.), chloroform was removed using a rotary evaporator. The residue was distilled under reduced pressure (110°C, 2 mmHg). Yield: 47.2 g, 55.8%.

CEO <sup>1</sup>H NMR (δ, ppm from trimethylsilane (TMS) in CDCl<sub>3</sub>): 0.90 (t, 3H,  $J_{\text{CH}_3\text{-CH}_2} = 7.5$  Hz,  $-\text{CH}_3$ ), 1.75 (q, 2H,  $J_{\text{CH}_3\text{-CH}_2} = 7.5$  Hz,  $-\text{CH}_2\text{-CH}_3$ ), 2.63 (t, 3H,  $J_{\text{CH}_2\text{-CH}_2} = 6.25$  Hz,  $-\text{CH}_2\text{-CH}_2\text{-CN}$ ), 3.63 (s, 2H,  $-\text{C}-\text{CH}_2\text{-O-}$ ), 3.72 (t, 3H,  $J_{\text{CH}_2\text{-CH}_2} = 6.25$  Hz,  $-\text{CH}_2\text{-CH}_2\text{-CN}$ ), 4.40 (dd, 4H,  $J_{\text{CH}_2\text{-O-CH}_2} = 6$  Hz, ring,  $-\text{CH}_2\text{-O-CH}_2\text{-}$ ).

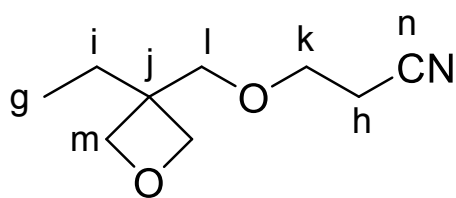
CEO <sup>13</sup>C NMR (δ, ppm from TMS in CDCl<sub>3</sub>): 5.5 ( $-\text{CH}_3$ ), 16.1 ( $-\text{CH}_2\text{-CH}_2\text{-CN}$ ), 23.6 ( $-\text{CH}_2\text{-CH}_3$ ), 40.6 ( $-\text{C-}$ ), 63.0 ( $-\text{CH}_2\text{-CH}_2\text{-CN}$ ), 71.1 ( $-\text{C}-\text{CH}_2\text{-O-}$ ), 75.5 ( $-\text{CH}_2\text{-O-CH}_2\text{-}$ , ring), 115.2 ( $-\text{CN}$ ).

(A)  $^1\text{H}$  NMR assignments



- (a) 0.90 (t, 3H,  $J = 7.5$  Hz)
- (b) 1.75 (q, 2H,  $J = 7.5$  Hz)
- (c) 2.63 (t, 3H,  $J = 6.25$  Hz)
- (d) 3.63 (s, 2H)
- (e) 3.72 (t, 3H,  $J = 6.25$  Hz)
- (f) 4.40, 4.45 (dd, 4H,  $J = 6$  Hz)

(B)  $^{13}\text{C}$  NMR assignments



- (g) 5.5
- (h) 16.1
- (i) 23.6
- (j) 40.6
- (k) 63.0
- (l) 71.1
- (m) 75.5
- (n) 115.2

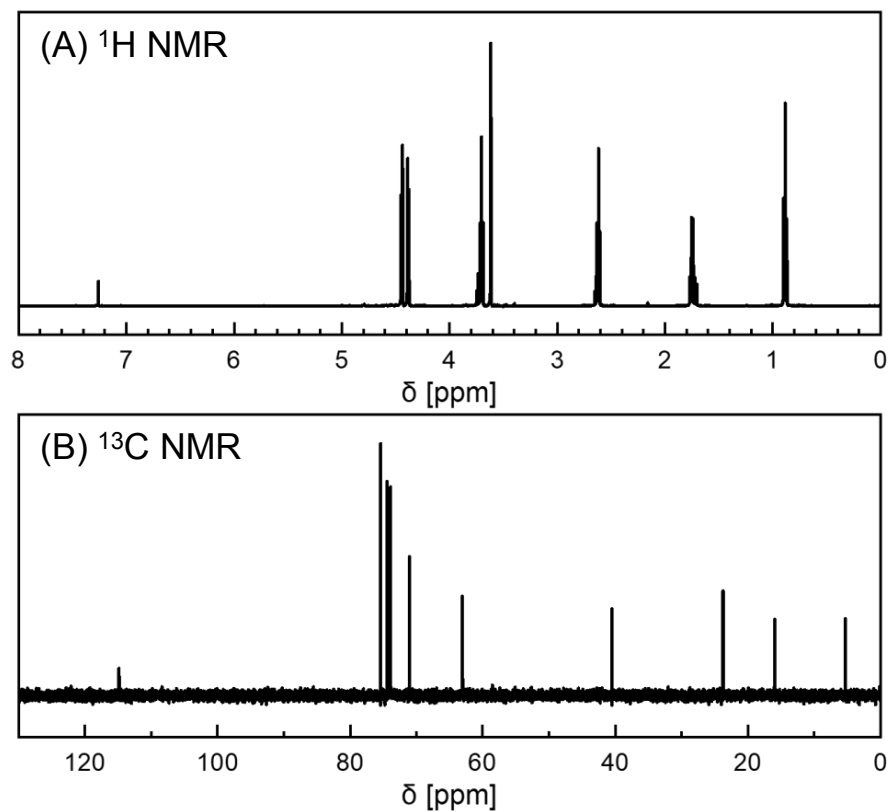


Figure S1 (A)  $^1\text{H}$  and (B)  $^{13}\text{C}$  NMR spectra of 3-(2-cyanoethoxymethyl)-3-ethyloxetane (CEO).

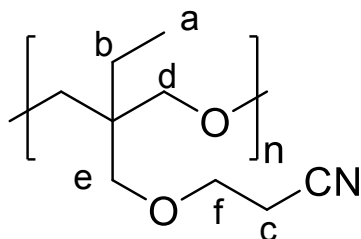
## Polymer synthesis

CEO were polymerized using a ring-opening cationic polymerization (ROCP) using boron trifluoride diethyl etherate ( $\text{BF}_3 \cdot \text{Et}_2\text{O}$ , Wako Pure Chemical. Co.) as an initiator. The molar ratio of the monomer (80 mmol) to the initiator (1.6 mmol) was fixed to 50 : 1. The monomer was dissolved in 1,2-dichloroethane followed by the addition of  $\text{BF}_3 \cdot \text{Et}_2\text{O}$  to the solution (total volume: 20 mL). The polymerization was performed under an Ar atmosphere at  $0^\circ\text{C}$  in a salt ice bath for 5 h. The ROCP was quenched using 10 mL of a  $4 \text{ mol dm}^{-3} \text{ NaCl}/1 \text{ mol dm}^{-3} \text{ NaOH}$  aqueous solution. Chloroform was then added to the resulting solution, and the mixture was washed with water. The organic phase containing the polyoxetanes was concentrated by rotary evaporation. The residual viscous solution was dropped into a 2-propanol reservoir to reprecipitate the polymerized CEO (PCEO). PCEO were finally collected by filtration using a glass filter and dried at  $70^\circ\text{C}$  under vacuum overnight (Yield 32.5%). The successful ROCP was further confirmed by  $^1\text{H}$  NMR as the disappearance of double-doublet signals ( $\delta = \sim 4.4\text{--}4.5$  ppm for the monomers) of methylene protons in the four-membered ring structure for the oxetane monomers.

PCEO  $^1\text{H}$  NMR ( $\delta$ , ppm from TMS in  $\text{CDCl}_3$ ): 0.85 (t, 3H,  $J_{\text{CH}_3-\text{CH}_2} = 7.5\text{Hz}$ ,  $-\text{CH}_3$ ), 1.39 (q, 2H,  $J_{\text{CH}_3-\text{CH}_2} = 7.5 \text{ Hz}$ ,  $-\text{CH}_2-\text{CH}_3$ ), 2.58 (t, 3H,  $J_{\text{CH}_2-\text{CH}_2} = 6.25 \text{ Hz}$ ,  $-\text{CH}_2-\text{CH}_2-\text{CN}$ ), 3.22 (s, 4H,  $-\text{C}-\text{CH}_2-\text{O}-$ ), 3.35 (s, 2H,  $-\text{C}-\text{CH}_2-\text{O}-$ ), 3.61 (t, 3H,  $J_{\text{CH}_2-\text{CH}_2} = 6 \text{ Hz}$ ,  $-\text{CH}_2-\text{CH}_2-\text{CN}$ )

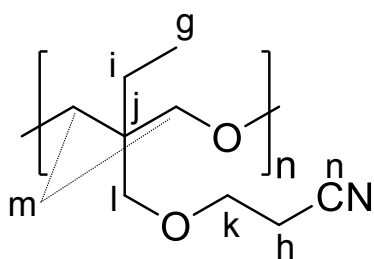
PCEO  $^{13}\text{C}$  NMR ( $\delta$ , ppm from TMS in  $\text{CDCl}_3$ ): 7.74 ( $-\text{CH}_3$ ), 18.8 ( $-\text{CH}_2-\text{CH}_2-\text{CN}$ ), 23.2 ( $-\text{CH}_2-\text{CH}_3$ ), 43.6 ( $-\text{C}-$ ), 66.0 ( $-\text{CH}_2-\text{CH}_2-\text{CN}$ ), 71.3 ( $-\text{C}-\text{CH}_2-\text{O}-$ ), 77.0 ( $-\text{CH}_2-\text{O}-\text{CH}_2-$ ), 118.2 ( $-\text{CN}$ ).

(A)  $^1\text{H}$  NMR assignments



- (a) 0.85 (t, 3H,  $J = 7.5$  Hz)
- (b) 1.39 (q, 2H,  $J = 7.5$  Hz)
- (c) 2.58 (t, 2H,  $J = 6$  Hz)
- (d) 3.22 (s, 4H)
- (e) 3.35 (s, 2H)
- (f) 3.61 (t, 2H,  $J = 6.25$  Hz)

(B)  $^{13}\text{C}$  NMR assignments



- (g) 7.74
- (h) 18.8
- (i) 23.2
- (j) 43.6
- (k) 66.0
- (l) 71.3
- (m) 77.0
- (n) 118.2

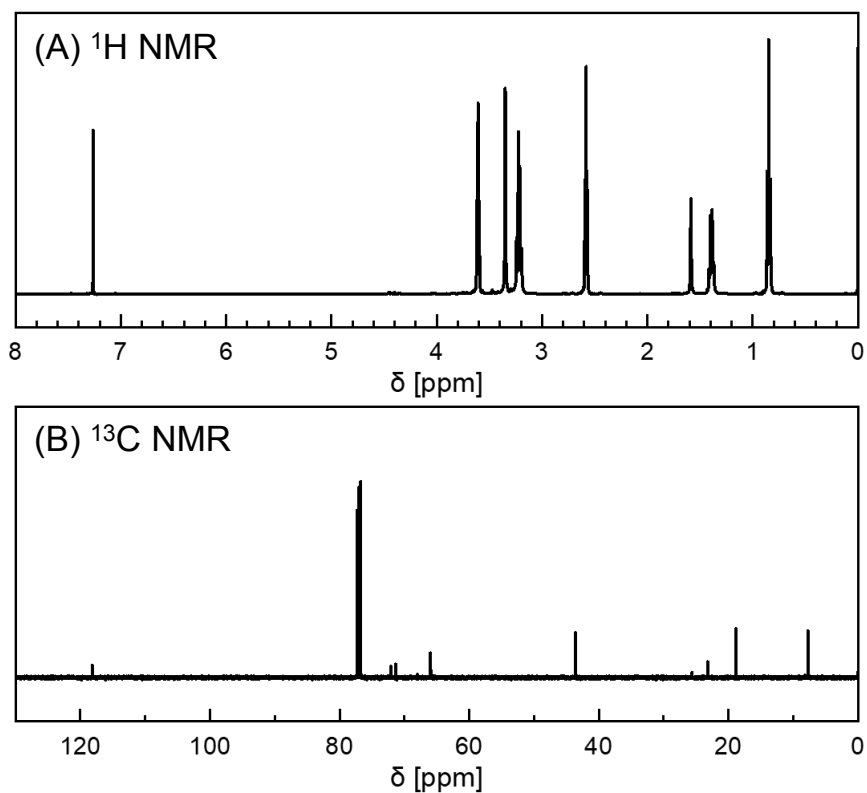


Figure S2 (A)  $^1\text{H}$  and (B)  $^{13}\text{C}$  NMR spectra of polymerized 3-(2-cyanoethoxymethyl)-3-ethyloxetane (PCEO).

## HEXTS measurement

High-energy X-ray total scattering (HEXTS) measurements were performed at room temperature with a high-energy X-ray diffraction apparatus (BL04B2 beamline at SPring-8, JASRI, Japan). The details of the measurements were similar to those described elsewhere.<sup>1-2</sup> The experimental X-ray structure factor,  $S^{\text{exp}}(q)$ , per stoichiometric volume, and radial distribution function,  $G^{\text{exp}}(r)$ , were calculated using equations (1) and (2), respectively.

$$S^{\text{exp}}(q) = \frac{\frac{I_{\text{coh}}(q)}{N} - \sum n_i f_i(q)^2}{[\sum n_i f_i(q)]^2} + 1 \dots (1)$$

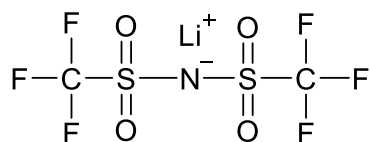
$$G^{\text{exp}}(r) - 1 = \frac{1}{2\pi^2 r \rho_0} \int_0^{q_{\text{max}}} q [S^{\text{exp}}(q) - 1] \sin(qr) \frac{\sin(q\pi/q_{\text{max}})}{q\pi/q_{\text{max}}} dq \dots (2)$$

where  $I_{\text{coh}}(q)$  is the corrected coherent scattering obtained from the observed X-ray scattering intensities.<sup>1-2</sup>  $n_i$  is the number of atoms  $i$  per stoichiometric volume. The parameters  $f_i$  and  $\rho_0$  represent the atomic scattering factor for atom  $i$  and the number density of atoms, respectively.

Table S1 Li salt concentration ( $c_{\text{Li}}$ ), density ( $d_{\text{MD}}$ ), compositions (number of ion-pairs and PCEO), and box length of the systems used for the MD simulation.

$a$	$c_{\text{Li}}$ [mol dm <sup>-3</sup> ]	$d_{\text{MD}}$ [g cm <sup>-3</sup> ]	Li-TFSI	PCEO	Box length
pure				60	5.170
1	3.121	1.481	480	60	6.292
3	1.533	1.198	160	60	5.654
10	0.554	1.070	48	60	5.335

(a) LiTFSI



(b) PCEO

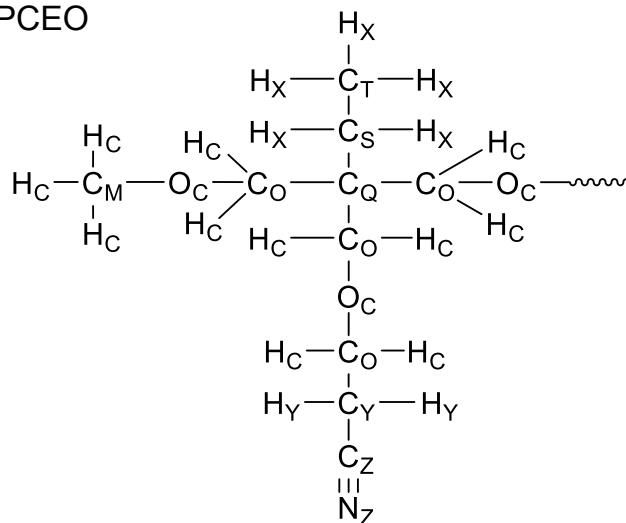


Figure S3 The structures of (a) LiTFSI and (b) PCEO with labels used in Table S2.

Table S2 OPLS-AA nonbonded parameters and atom types for Li<sup>+</sup>, TFSI<sup>-</sup>, and PCEO.

	atom	$\epsilon$ [kcal mol <sup>-1</sup> ]	$\sigma$ [Å]	$q$ [e]
Li	Li	0.191	1.460	1.000
TFSI	N	0.170	3.250	-0.660
	S	0.250	3.550	1.020
	O	0.210	2.960	-0.530
	F	0.053	2.950	-0.160
	C	0.066	3.500	0.350
PCEO	C <sub>M</sub>	0.066	3.500	0.098
	C <sub>O</sub>	0.066	3.500	0.140
	C <sub>Q</sub>	0.066	3.500	0.000
	C <sub>S</sub>	0.066	3.500	-0.120
	C <sub>T</sub>	0.066	3.500	-0.180
	C <sub>Y</sub>	0.066	3.300	-0.080
	C <sub>Z</sub>	0.150	3.650	0.460
	O <sub>C</sub>	0.140	2.900	-0.400
	H <sub>C</sub>	0.030	2.500	0.034
	H <sub>X</sub>	0.030	2.500	0.064
	H <sub>Y</sub>	0.015	2.500	0.064
	N <sub>Z</sub>	0.170	3.200	-0.560



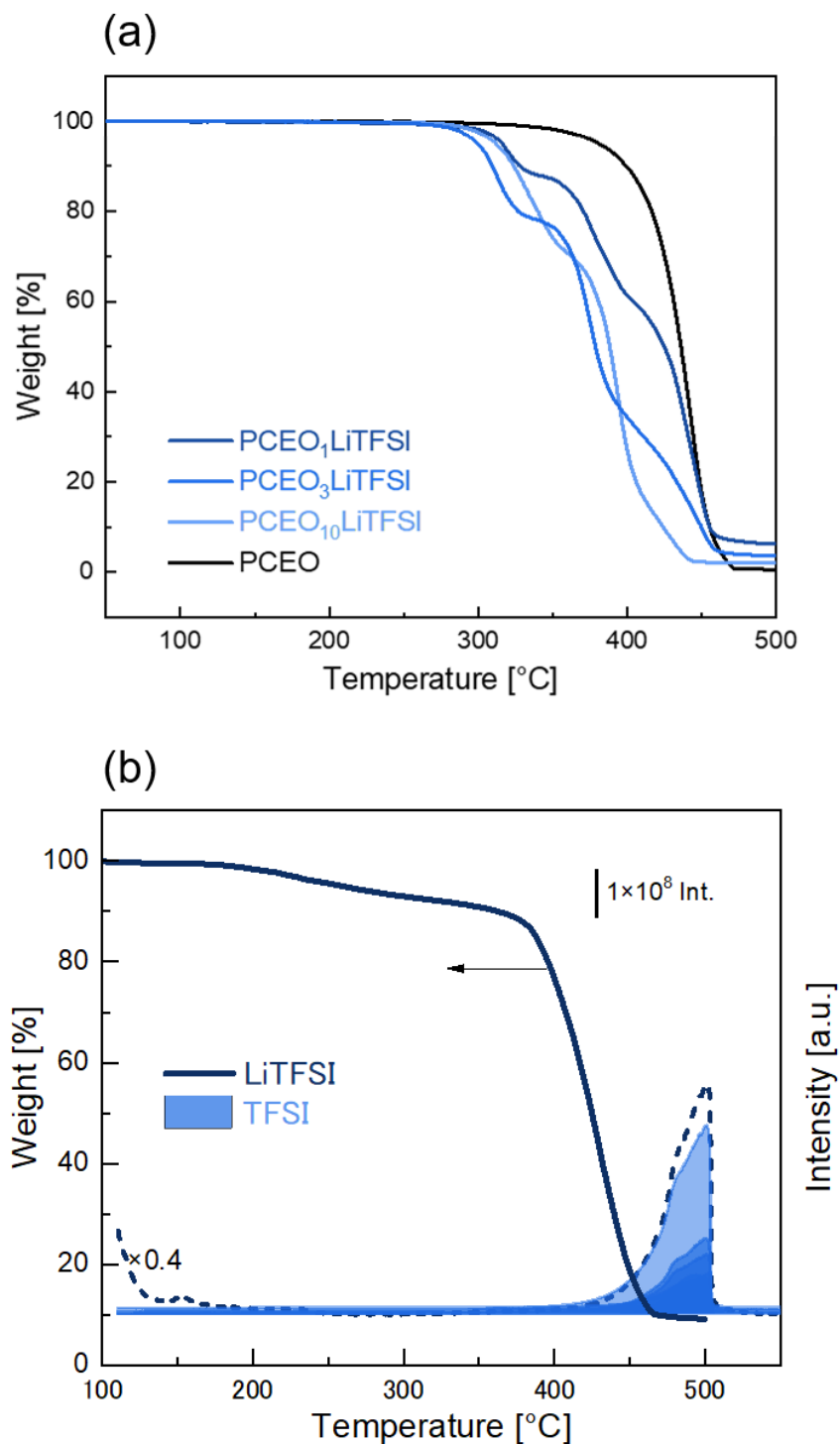


Figure S4 (a) Thermogravimetry (TG) curves for pristine PCEO and  $\text{PCEO}_a\text{LiTFSI}$  electrolytes ( $a = 1, 3, \text{ and } 10$ ). (b) thermogravimetry (TG) curves and corresponding mass spectrometry (MS) analysis for pure LiTFSI. TG curve was obtained under He atmosphere at a heating rate of  $20^\circ\text{C min}^{-1}$  after each sample was pre-heated at  $150^\circ\text{C}$  for 10 min. Detected MS fragment ( $m/z = 48, 64, 69, 85$ ) was assigned to TFSI. Broken line shows overall MS curve.

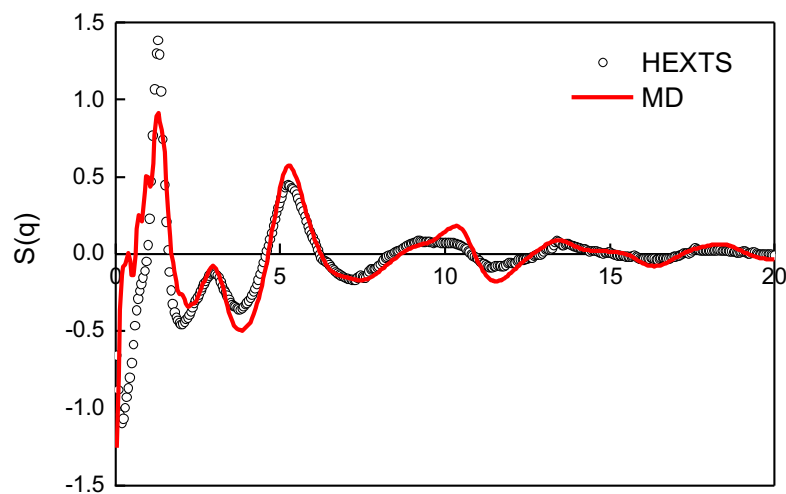


Figure S5 Structure factor in the form  $S(q)$  for  $\text{PCEO}_3\text{LiTFSI}$  obtained from high-energy X-ray total scattering (HEXTS) measurements (open circles) and all-atom molecular dynamics (MD) simulations (continuous red lines).

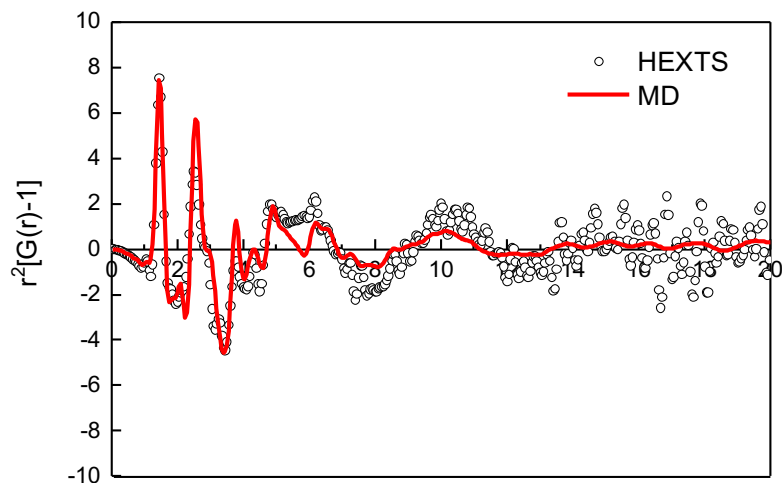


Figure S6 Difference radial distribution functions in the  $r^2 [G(r) - 1]$  for  $\text{PCEO}_3\text{LiTFSI}$  obtained from high-energy X-ray total scattering (HEXTS) measurements (open circles) and all-atom molecular dynamics (MD) simulations (continuous red lines). The  $G(r)$  functions were calculated by Fourier transformation of the corresponding structure factors,  $S(q)$ .

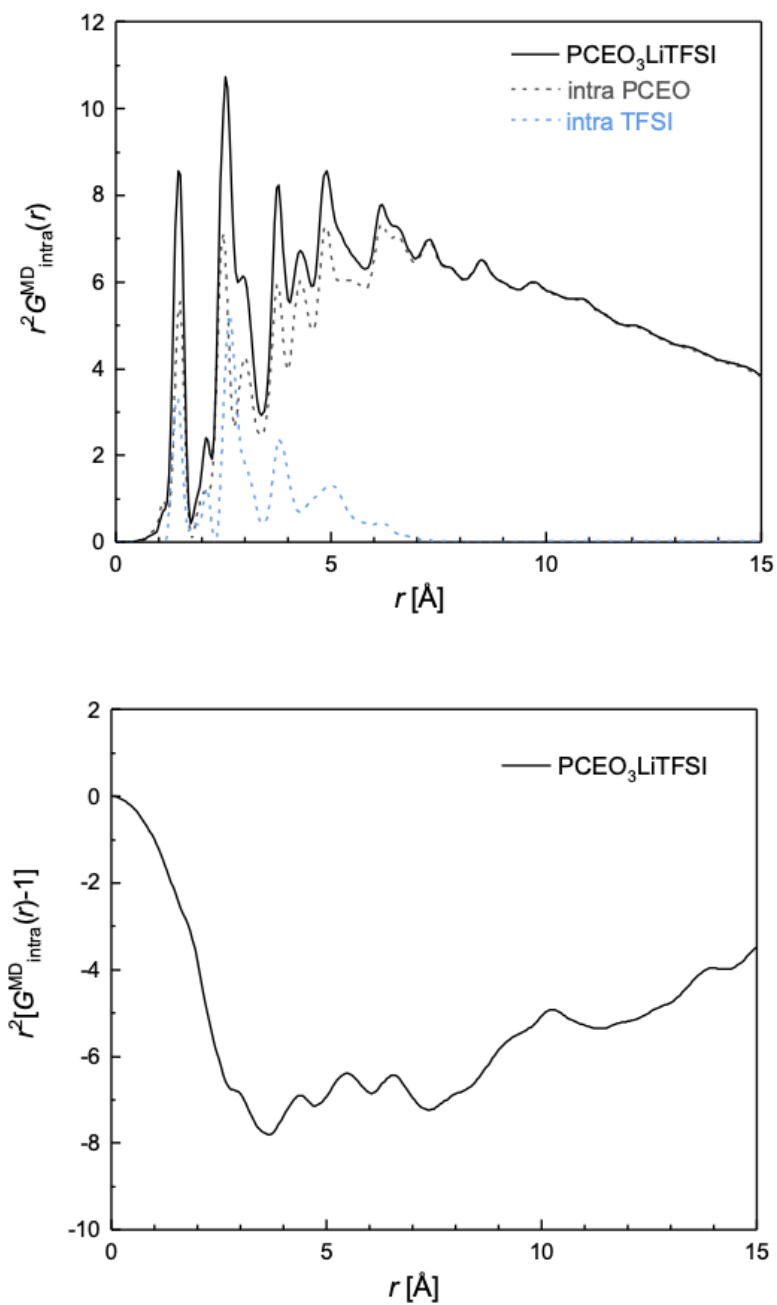


Figure S7 Partial  $G^{\text{MD}}(r)$ s for typical (a) intramolecular and (b) intermolecular contributions in  $\text{PCEO}_3\text{LiTFSI}$  electrolyte.

Table S3 IR peak area ratio of bound-CN obtained from the deconvoluted  $\nu(\text{C}\equiv\text{N})$  peak. The estimated coordination number for  $\text{PCEO}_a\text{LiTFSI}$  ( $a = 1, 3$ , and  $10$ ) based on bound-CN peak ratio is also shown.

<b>a</b>	<b>Peak area ratio of bound C<math>\equiv</math>N [%]</b>	<b>Estimated coordination number</b>
1	94.23	0.94
3	76.29	2.29
10	35.78	3.58

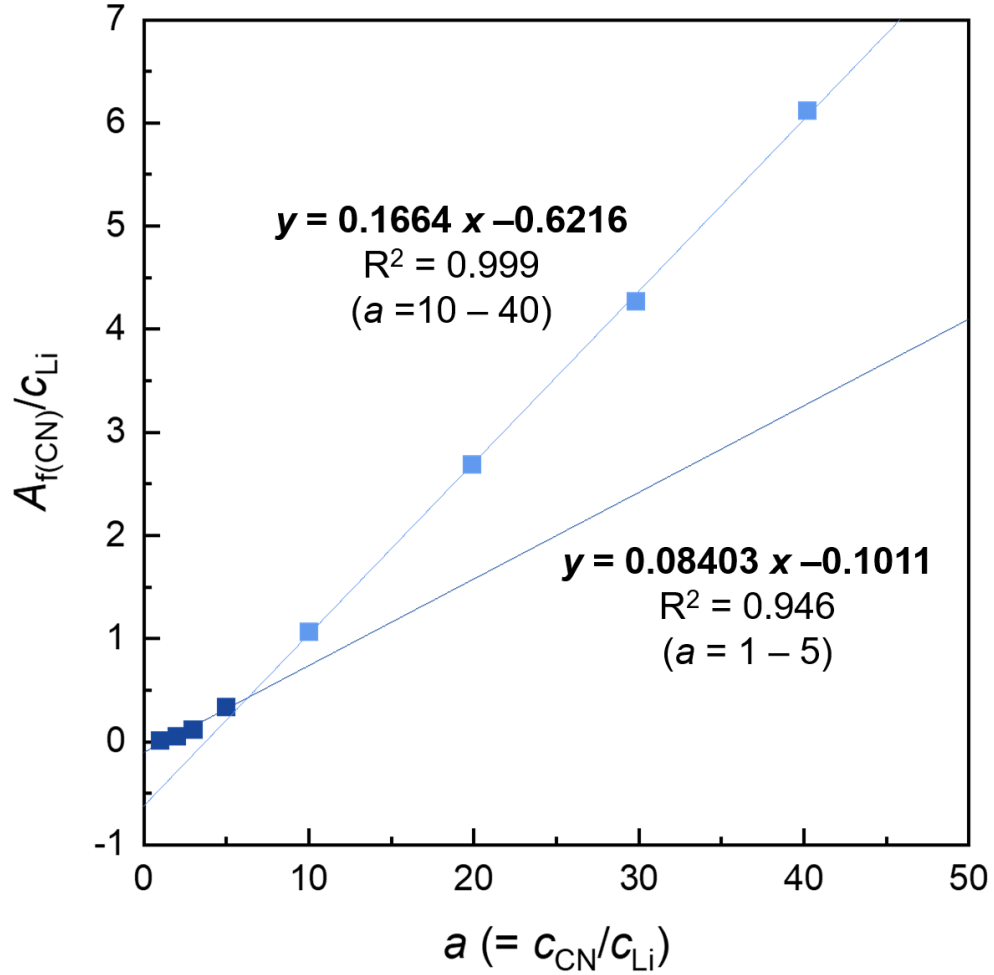


Figure S8  $A_{f(CN)}/c_{Li}$  plotted as a function of salt concentration  $a (= c_{CN}/c_{Li})$  for  $PCEO_aLiTFSA$ . The solid line represents the least-square linear fitting to obtain  $J_{f(CN)}$  and  $N^{IR}$  from the slope and the intercept, respectively. The linear least-square fitting for low concentration region ( $a = 10-40$ ) and high concentration region ( $a = 1-5$ ) provided average  $N^{IR}$  of 3.74 and 1.20, respectively, based on the following relationship,

$$\frac{A_{f(CN)}}{c_{Li}} = \varepsilon_{f(CN)} \left( \frac{c_{CN}}{c_{Li}} - N^{IR} \right) = \varepsilon_{f(CN)} (a - N^{IR}).$$

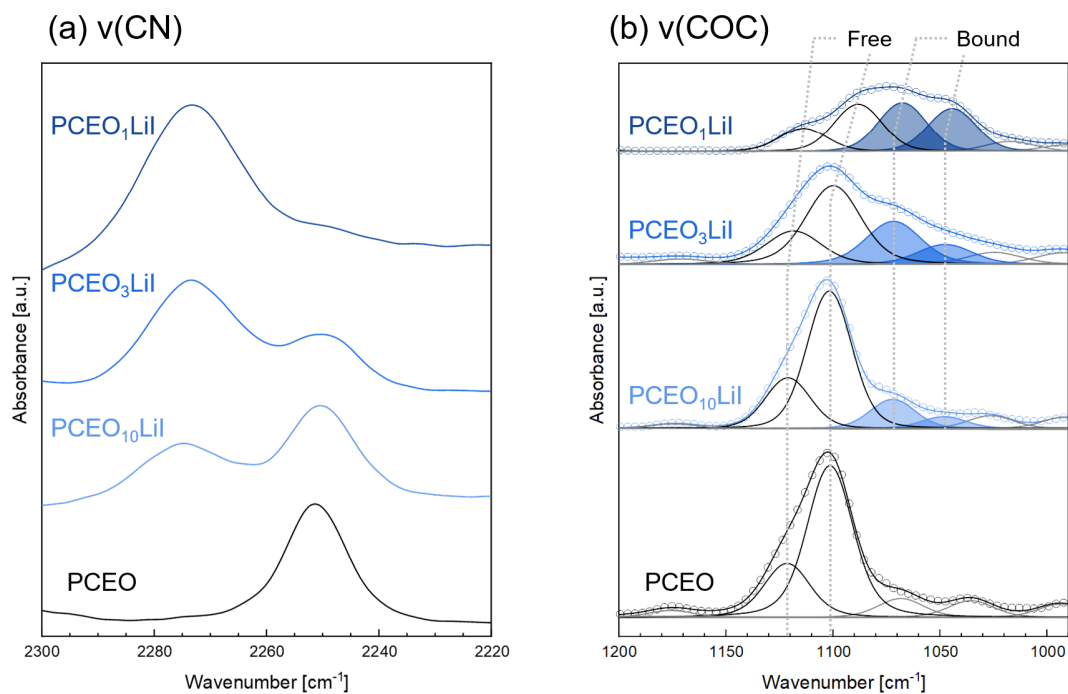


Figure S9 ATR-FTIR spectra (open circle) and typical curve-fitting results (solid line) of (a)  $\nu(\text{CN})$  and (b)  $\nu_{\text{as}}(\text{COC})$  for pristine PCEO and PCEO<sub>a</sub>LiI electrolytes ( $a = 1, 3$ , and  $10$ ) in the frequency range of (a)  $2220\text{--}2300\text{ cm}^{-1}$  and (b)  $990\text{--}1200\text{ cm}^{-1}$  at room temperature. Peak deconvolution was performed by PeakFit software using pseudo-Voigt functions with fixed half-width at half-maximum.

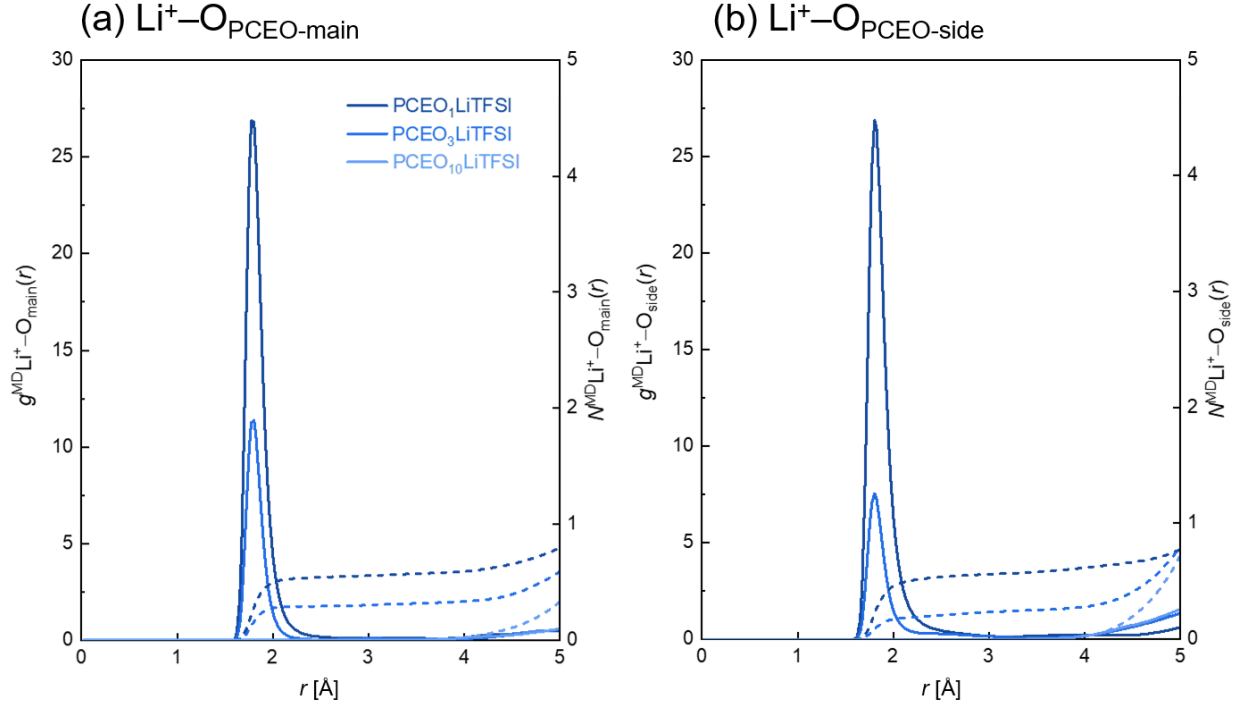


Figure S10 Atom-atom pair correlation functions ( $g^{\text{MD}}_{\text{Li}-\text{X}}(r)$ : left axis, solid lines) and corresponding integrated profiles (coordination number  $N^{\text{MD}}_{\text{Li}^+-\text{X}}(r)$ : right axis, broken lines] for (a)  $\text{Li}^+-\text{O}_{\text{PCEO-main}}$  and (b)  $\text{Li}^+-\text{O}_{\text{PCEO-side}}$  for  $\text{PCEO}_a\text{LiTFSI}$  ( $a = 1, 3, \text{ and } 10$ ) electrolytes.

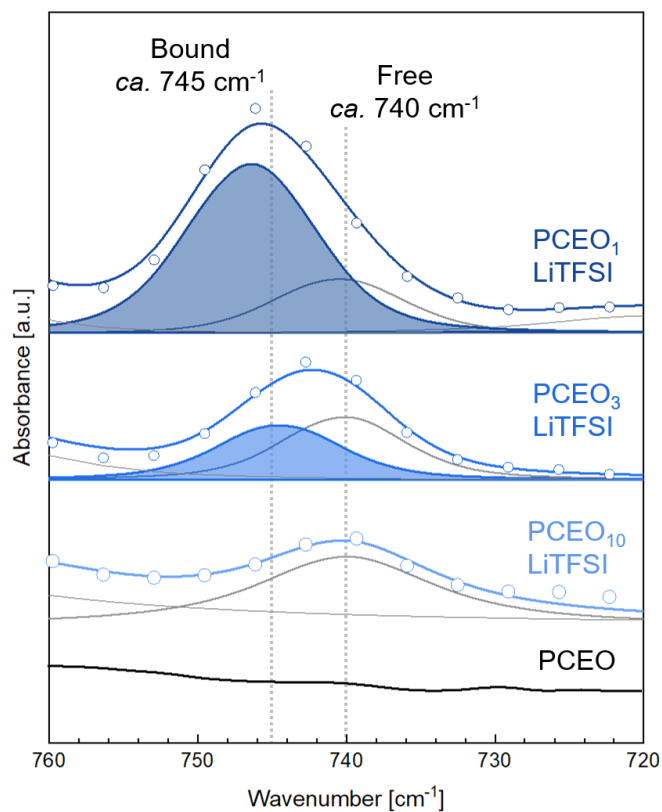


Figure S11 ATR-FTIR spectra (open circle) and typical curve-fitting results (solid line) of  $\text{CF}_3$  bending vibration for pristine PCEO and  $\text{PCEO}_a\text{LiTFSI}$  electrolytes ( $a = 1, 3$ , and  $10$ ) in the frequency range of  $720\text{--}760\text{ cm}^{-1}$  at room temperature. Peak deconvolution was performed by PeakFit software using pseudo-Voigt functions with fixed half-width at half-maximum.



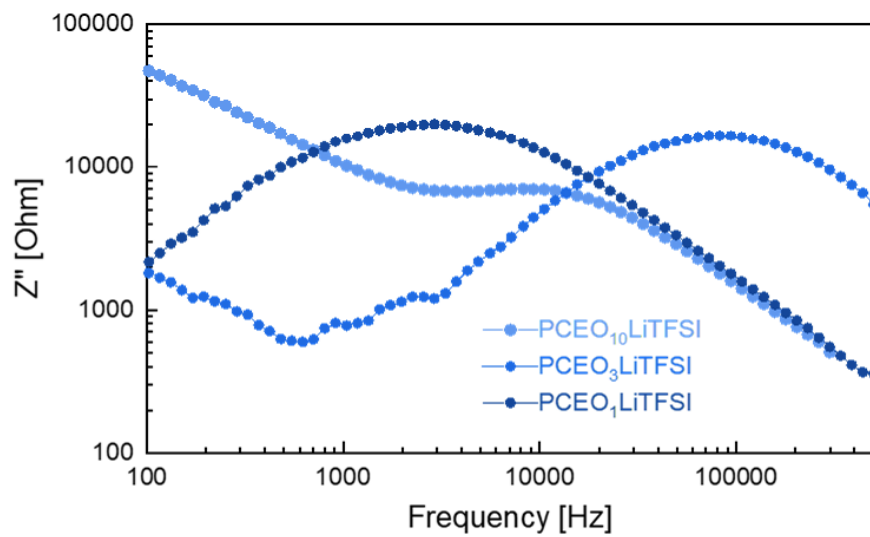


Figure S12 Frequency dependence of imaginary impedance ( $Z''$ ) for  $\text{PCEO}_a\text{LiTFSI}$  ( $a = 1, 3$ , and  $10$ ) electrolytes during EIS measurement with the conductivity cell  $[\text{SS} \mid \text{electrolytes} \mid \text{SS}]$  measured at open circuit potential with amplitude of  $10 \text{ mV}$  at  $70^\circ\text{C}$ .

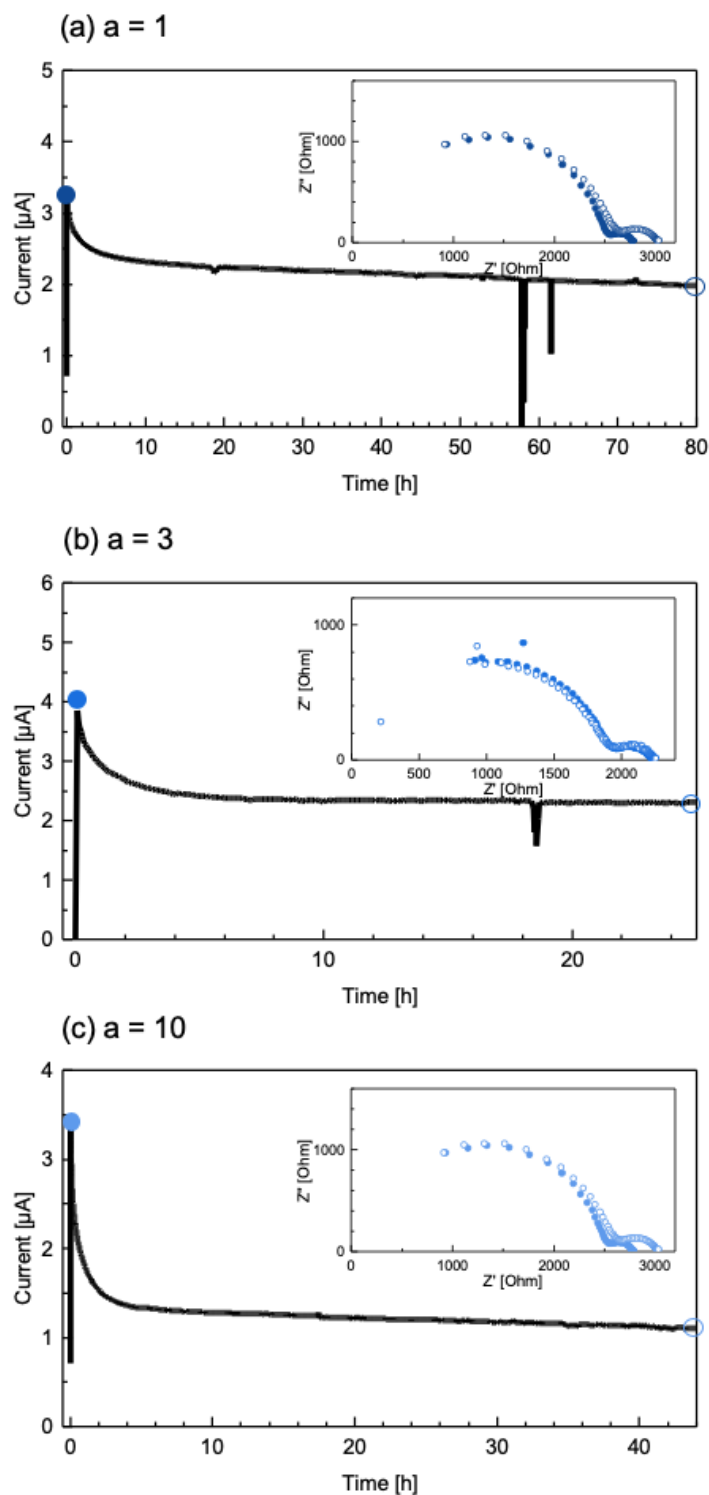
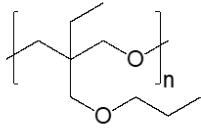


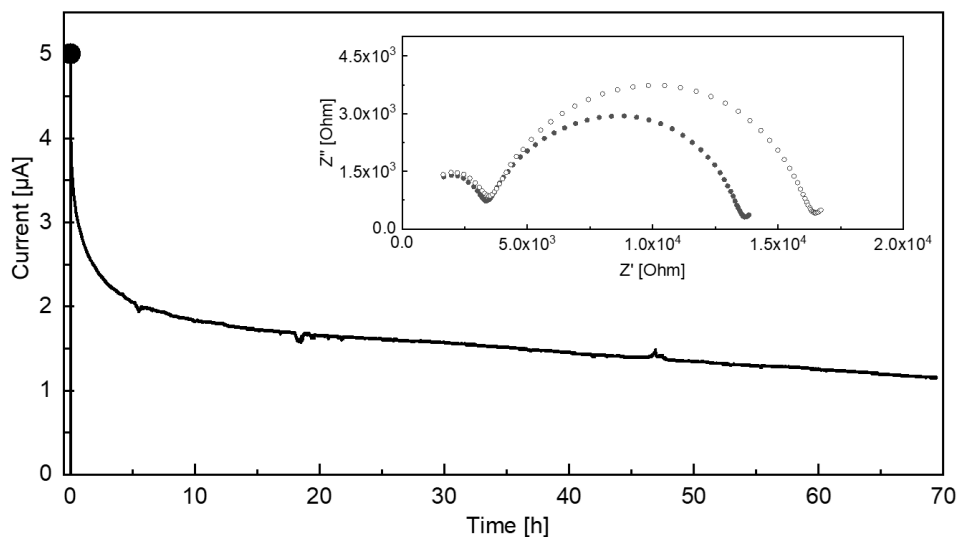
Figure S13 Time dependence of DC polarization and corresponding nyquist plots before and after polarization used to calculate the transference number for  $\text{PCEO}_a\text{LiTFSI}$  ( $a = 1, 3$ , and  $10$ ). EIS measurement was performed using the symmetric cell of  $[\text{Li metal} | \text{polymer electrolyte} | \text{Li metal}]$  at  $70^\circ\text{C}$ .

Table S4 Measured parameter used to calculate the transference number for  $\text{PCEO}_a\text{LiTFSI}$  ( $a = 1, 3, \text{ and } 10$ ) and the corresponding calculated values of  $\text{Li}^+$  transference numbers at  $70^\circ\text{C}$ .

	$I_0$ [ $\mu\text{A}$ ]	$I_s$ [ $\mu\text{A}$ ]	Frequency [Hz]				$\Delta V$ [mV]	$t_{\text{Li}^+}$
			$R_e^i$ [ $\Omega$ ]	$R_e^f$ [ $\Omega$ ]	$R_l^i$ [ $\Omega$ ]	$R_l^f$ [ $\Omega$ ]		
$\text{PCEO}_1\text{LiTFSI}$	3.214	1.982	6309.67		1		10	0.70
			2863.2	3227.0	112.3	197.5		
$\text{PCEO}_3\text{LiTFSI}$	3.861	2.313	166807		27.8		10	0.58
			1966.6	1974.1	266.8	272.4		
$\text{PCEO}_{10}\text{LiTFSI}$	3.370	1.110	7943.0		1		10	0.33
			2537.3	2631.9	246.7	399.7		

Table S5 Molecular weight ( $M_n$ , number average and  $M_w$ , weight average) of the synthesized PBuEO polymer.

PBuEO	Molecular weight		
	$M_n$ [g mol <sup>-1</sup> ]	$M_w$ [g mol <sup>-1</sup> ]	$M_w/M_n$ [-]
	$5.66 \times 10^4$	$1.06 \times 10^5$	1.86



	$I_0$ [μA]	$I_s$ [μA]	$R_e^i$ [Ω]	$R_e^f$ [Ω]	$R_l^i$ [Ω]	$R_l^f$ [Ω]	$\Delta V$ [mV]	$t_{Li+}$
PBuEO <sub>3</sub> LiTFSI	5.095	1.300	3129	3198	10693	13429	10	0.14

Figure S14 Time dependence of DC polarization and corresponding nyquist plots before and after polarization used to calculate the transference number for PBuEO<sub>a</sub>LiTFSI ( $a = 3$ ). EIS measurement was performed using the symmetric cell of [Li metal | polymer electrolyte | Li metal] at 70°C. The measured parameter and obtained transference number for PBuEO<sub>a</sub>LiTFSI ( $a = 3$ ) is summarized below the graph.

## References

1. Kamiyama, Y.; Shibata, M.; Kanzaki, R.; Fujii, K., *Phys. Chem. Chem. Phys.* **2020**, 22 (10), 5561-5567.
2. Sogawa, M.; Sawayama, S.; Han, J.; Satou, C.; Ohara, K.; Matsugami, M.; Mimura, H.; Morita, M.; Fujii, K., *J. Phys. Chem. C* **2019**, 123, 8699-8708.